Journal of the Korean Nuclear Society
Volume 30, Number 3, pp.273~286, June 1998

《Technical Note》

Analysis of High Burnup Fuel Behavior Under Rod Ejection Accident in the Westinghouse-Designed 950 MWe PWR

Chan Bock Lee and Byung Oh Cho
Korea Atomic Energy Research Institute
150 Dukjin-dong, Yusong-gu, Taejon 305-353, Korea

Oh Hwan Kim, Young Baik Kim, and Jin Gon Chung
Korea Nuclear Fuel Company
150 Dukjin-dong, Yusong-gu, Taejon 305-353, Korea

(Received July 27, 1996)

Abstract

As there has arisen a concern that failure of the high burnup fuel under the reactivity-insertion accident(RIA) may occur at the energy lower than the expected, fuel behavior under the rod ejection accident in a typical Westinghouse-designed 950 MWe PWR was analyzed by using the three dimensional nodal transient neutronics code, PANBOX2 and the transient fuel rod performance analysis code, FRAP-T6. Fuel failure criteria versus the burnup was conservatively derived taking into account available test data and the possible fuel failure mechanisms. The high burnup and longer cycle length fuel loading scheme of a peak rod burnup of 68 MWD/kgU was selected for the analysis. Except three dimensional core neutronics calculation, the analysis used the same core conditions and assumptions as the conventional zero dimensional analysis. Results of three dimensional analysis showed that the peak fuel enthalpy during the rod ejection accident is less than one third of that calculated by the conventional zero dimensional analysis methodology and the fraction of fuel failure in the core is less than 4 %. Therefore, it can be said that the current design limit of less than 10 percent fuel failure and maintaining the core coolable geometry would be adequately satisfied under the rod ejection accident, even though the conservative fuel failure criteria derived from the test data are applied.

1. Introduction

Performance of the high burnup fuel under the rod ejection accident in the PWR has recently been of great concern as some of the simulated RIA test results in the research reactors as shown in Fig. 1 indicated that there might be a need to revise the current fuel failure criteria[1]

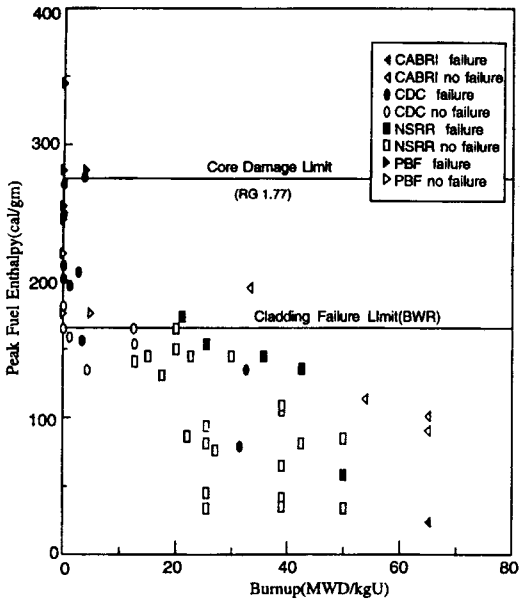

Fig. 1. Simulated RIA Test Results in the Research Reactors.

which had been determined based upon the test results of the unirradiated fuel rods. Specifically, results of CABRI tests[2] raised the concern that the failure threshold of the high burnup fuel may be significantly decreased due to the degradation of the fuel properties at high burnup.

It can be said that the current analysis methodology of the rod ejection accident in the PWR employs a significant conservatism since the uncertainties in the prediction of neutronics and transient fuel behavior were compensated by allowing the conservatism as much as the consequence of the accident is within the allowable safety limit. However, as there was an indication that the current design criteria on the fuel behavior under the rod ejection accident need to be revised, a need to re-analyze the current analysis methodology and remove reasonably the over-conservatism has arisen. The primary area for that is the transient neutronics prediction where zero dimensional analysis is employed. The improvement of the neutronics code and computing power made it possible to simulate the entire transient core three dimensionally. This realistic prediction could significantly decrease the over-conservatism in the prediction of transient core power.

In this study, the three dimensional core behavior under the rod ejection accident with same conservative assumptions used in the conventional zero dimensional analysis will be performed and the fuel failure criteria based upon the currently available test results will be newly derived and applied to check whether the results of the conventional analysis is still bounding.

2. Fuel Behavior Analysis Under Rod Ejection Accident

2.1. Three Dimensional Analysis Methodology

Safety analysis of rod ejection accident can be divided largely into three steps such as transient power calculation, fuel behavior analysis and radiological consequence analysis. The current fuel design criteria under the rod ejection accident in the pressurized water reactor is that the maximum radially averaged fuel pellet enthalpy for the irradiated fuel is less than 200 cal/gm to prevent the core damage and the fuel would fail if DNB occurs during the transient. The safety analysis results by the conventional analysis methodology showed that the fractional fuel failure was less than 10 % and the core damage was prevented. Results of the radiological consequence analysis in the safety analysis report with the assumption of 10 % fuel failure were well within the safety limit.

Fig. 2 shows the analysis flow diagram of the rod ejection accident analysis in this study. At

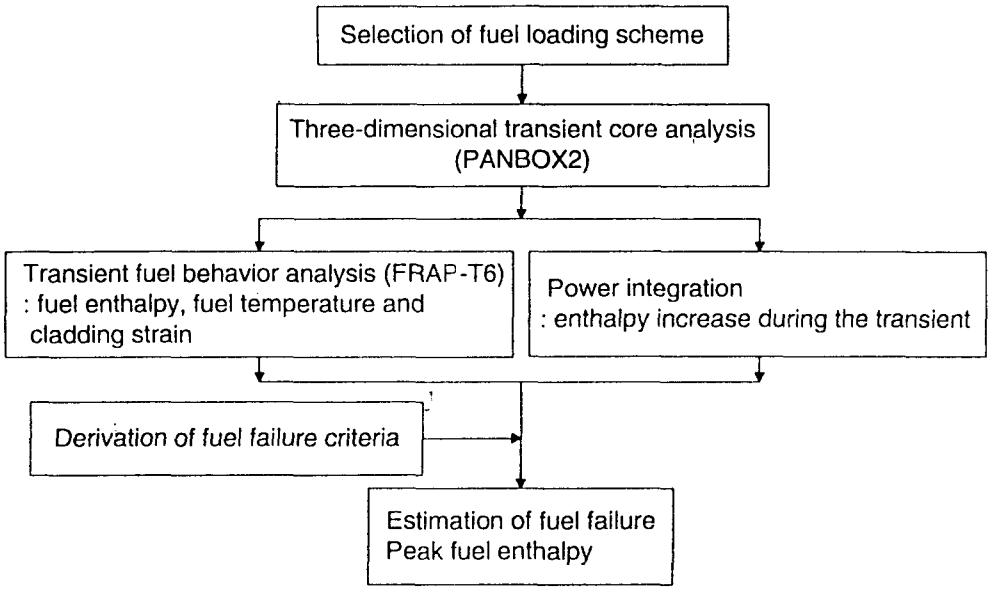

Fig. 2. Analysis Flow Diagram of the Rod Ejection Accident.

first, the relevant core loading pattern is selected for the analysis and neutronics calculation of the transient was then performed by the PANBOX2 code[3] to predict the core and the fuel rod power change during the transient. The PANBOX2 code was validated through the comparison with the several benchmark results calculated by other transient neutronics code such as PANTHER [4]. Then, the fuel rod behavior during the transient was predicted with the rod power histories from PANBOX2 code by FRAP-T6[5] which was validated by comparing with the in-reactor test results including the RIA test results.

Transient fuel behavior is then interpreted in terms of such fuel performance parameters as fuel temperature and enthalpy, and cladding stress and strain which FRAP-T6 can predict. To estimate the fuel enthalpy increase during the transient for all the rods the transient power histories were simply integrated by assuming that the heat generated in the fuel during the transient was not released out of the fuel at all since the transient ends in less than 0.4 sec for the HZP case and it ends in less than 2.0 sec for the HFP case. Figs. 3 and 4 compares the enthalpy increase calculated by the power integration method with the results of FRAP-T6 prediction for the HZP and the HFP cases. It can be seen that the differences are about 15 to 22 % for the HZP case and about 40 to 60 % for the HFP case. The difference depends directly upon both the duration of the transient and the gap conductance during the transient which controls the heat transfer out of the fuel pellet. Anyhow, the power integration method over-estimates the fuel enthalpy increase during the transient by at least 15 % and therefore is conservative.

Finally, the amount of the fuel failure will be estimated by comparing the calculated results of the enthalpy increase with the newly derived fuel

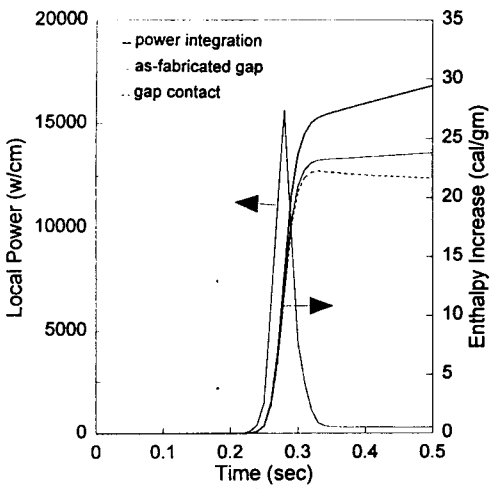

Fig. 3. Comparison of the Enthalpy Increase Predicted by the FRAP-T6 with That by the Power Integration Method for the HZP Case.

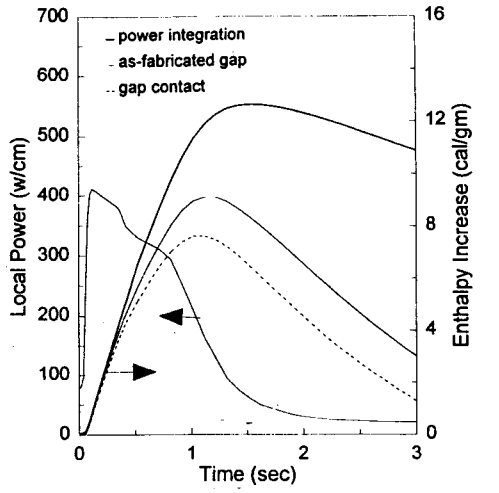

Fig. 4. Comparison of the Enthalpy Increase Predicted by the FRAP-T6 with That by the Power Integration Method for the HFP Case.

Table 1. Core Conditions and Assumptions in the Rod Ejection Accident Analysis.

Item	Core conditions / Assumptions
- Burnup step	- End of cycle
- Rod ejection time	- 0.1 sec
- Initial power level	- HZP (1 watt), HFP (102 % full power)
- Initial bank position	- Rod insertion limit - 12 steps (at given power level)
- Final bank position	- Only the stuck rod is ejected from initial bank position
- Axial offset	- For HFP : reference axial offset + right limit of the target axial offset For HZP : HFP xenon distribution is used.
- Xenon status	- Bottom peaked xenon distribution
- Absorption cross section of the ejected control rod	- Increased by 20 %
- Delayed neutron fraction	- Decreased by 10 %

failure criteria. The fuel failure criteria will be revised considering the available test results and the possible fuel failure mechanism.

2.2. Transient Power Calculation

To predict the core and the fuel rod power distributions during the rod ejection transient, PANBOX2 code was used with a node per fuel assembly in the half core simulation. PANBOX2 code is a nodal transient neutronics code coupled with a thermal-hydraulic dynamics code, COBRA and solves the space-time dependent neutron diffusion equation using nodal expansion method (NEM) and/or nodal integration method (NIM). To conservatively evaluate the transient power variation the core conditions and assumptions in this analysis are

kept identical to those in the conventional design methodology, as shown in Table 1. The only difference is that three dimensional analysis is used instead of conventional zero dimensional analysis. Transient power level depends strongly on the ejected rod worth which is a function of the absortion capability of the ejected control rod and the delayed neutron fraction. Therefore, conservatism is given by decreasing 10 percent for the delayed neutron fraction and increasing 20 percent for the absorption capability of the ejected control rod.

Analysis of the various fuel loading patterns in the Westinghouse-designed 950 MWe plant core showed that fresh or once burned fuel assemblies are more likely located in the D-bank position where a control rod is conservatively assumed to be ejected, and twice or thrice burned fuel assemblies can be located next to the D-bank position. Then, the ultra low leakage and 18 month cycle length fuel loading scheme with a peak rod burnup of 68 MWD/kgU was selected for the analysis.

The transient Pin Maximum Linear Heat Generation Rate (PMLHGR) of all the fuel rods in the core after rod ejection is determined from the transient core power level and total pin peaking factor, Fq values as follows:

$$PMLHGR(t) = ALHGR \times P(t) \times F_q$$

where,

$ALHGR$ = average linear heat generation rate (w/cm)

F_q = total pin peaking factor (Fxyz) including uncertainties and technical tolerances

$P(t)$ = instant core power level

2.3. Derivation of Fuel Failure Criteria

Fuel rod behavior under the rod ejection accident was predicted by the fuel transient code FRAP-T6 using the rod power histories generated by PANBOX2 code. The performance parameters of concern were fuel centerline temperature, pellet enthalpy and the cladding strain. Figs. 5 and 6 illustrate the transient fuel rod power, fuel enthalpy, fuel centerline temperature and the cladding strain predicted by the FRAP-T6 code during the rod ejection transients for the HZP and the HFP cases, respectively. They show that the width (in FWHM) of the transient power pulse is about 35 msec for the HZP case and about 0.8 sec for the HFP case, and fuel enthalpy and cladding strain increase in a very short time.

Fuel failure limit currently used in the reactivity insertion accident(RIA) analysis is based upon the test results of unirradiated and irradiated-to-low burnup fuels, such that occurrence of departure from nucleate boiling(DNB) is assumed as fuel failure limits in PWR and occurrence of dryout or radial average fuel enthalpy rise of 170 cal/gm is used in BWR. However, as shown in Fig. 1, some test results such as CDC (peak fuel enthalpy at fuel failure, 85 cal/gm)[1], NSRR HBO-1 (peak fuel enthalpy at fuel failure, 60 cal/gm)[6] and CABRI Na-1 (peak fuel enthalpy at fuel failure, 30 cal/gm)[2] indicated that failure of the irradiated fuel under RIA may occur at the energy lower than the current limits by PCMI(pellet cladding mechanical interaction) due to reduction of cladding ductility and fuel gap width.

Cladding ductility is a key parameter in determining occurrence of fuel failure by PCMI. When the cladding ductility is sufficient, fuel failure has not occurred up to the plastic deformation of 2 ~ 3 %. However, in CABRI Rep. Na-1 test[7] fuel failure occurred at very low cladding strain, which seems to have resulted from a significant reduction of cladding

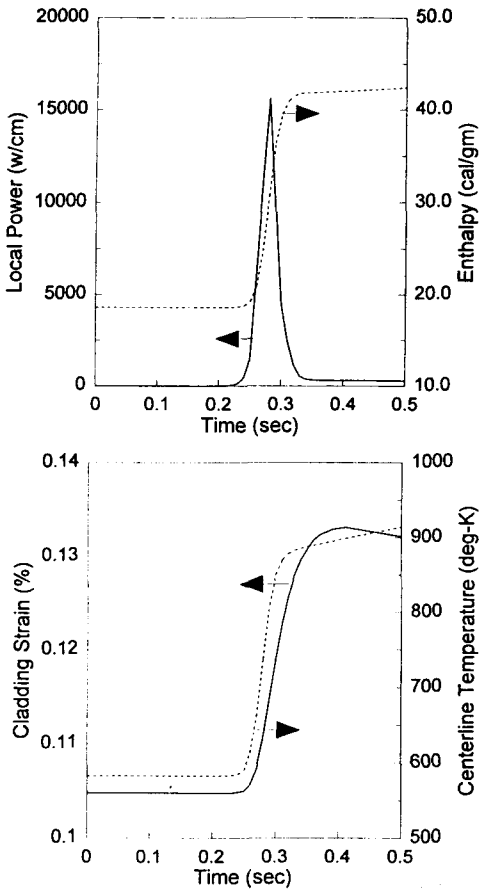

Fig. 5. Predicted Transient Fuel Behavior During the HZP Rod Ejection Transient at EOC.

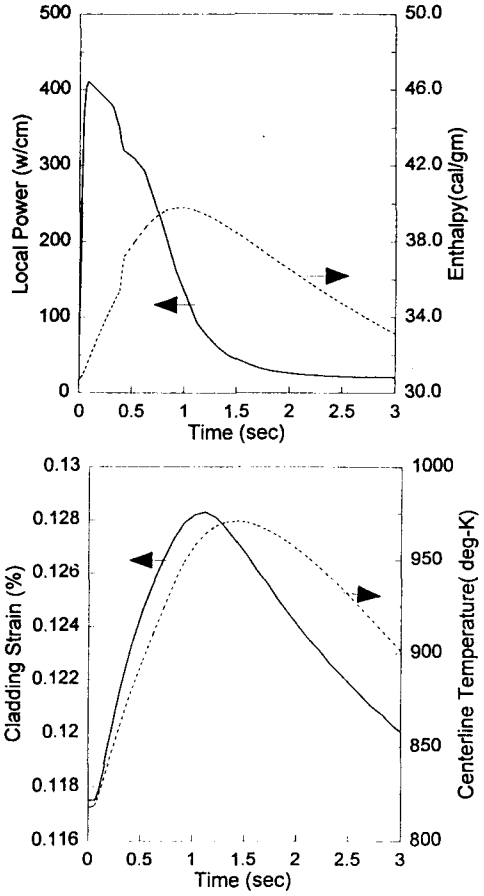

Fig. 6. Predicted Transient Fuel Behavior During the HFP Rod Ejection Transient at EOC.

ductility by oxide spallation and subsequent local hydride concentration. In other CABRI tests[7] such as Rep. Na-4 (peak fuel enthalpy 95 cal/gm) and Rep. Na-5 (peak fuel enthalpy 105 cal/gm), fuel specimens of the same burnup of 63 MWD/kgU as Rep. Na-1 test were used, but have not failed. It strongly indicates that the effect of pellet rim in the high burnup fuel upon the fuel failure under the RIA condition is not significant. Cladding ductility depends upon many variables such as corrosion, hydrogen concentration, fast neutron fluence and strain rate, etc.. However, for the application to the RIA analysis it is desirable to set cladding ductility versus burnup. Fast neutron fluence increases with in-core residence period and hydrogen content of the cladding increases with cladding corrosion. Hydrogen in the cladding tends to diffuse into the lower temperature region by thermal diffusion such that hydrogen concentration in the lower temperature region between the pellets is higher than the other region. In particular, when the oxide spallation occurred locally, thermal resistance of the oxide removed and then the temperature decreases significantly in that region so that hydrogen concentration increases locally. Test results[8] showed that local hydride concentration after oxide spallation reduced the cladding ductility significantly.

Cladding strain by PCMI depends upon not only the fuel enthalpy increase but also the fuel

Table 2. Tentative Fuel Failure Limits Based upon the Published Test Results.

Initial condition	Burnup(MWD/kgU)	Fuel failure limit
HZP	0 ~ 30	DNB or total fuel enthalpy 85 cal/gm
	> 30	fuel enthalpy increase 15 cal/gm
HFP	0 ~ 30	DNB or total fuel enthalpy 85 cal/gm
	> 30	fuel enthalpy increase 7 cal/gm

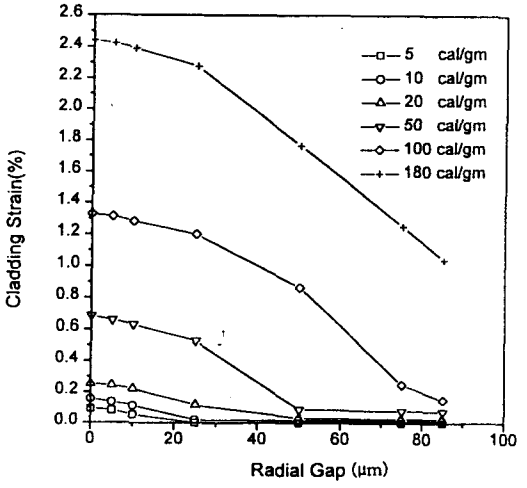

Fig. 7. Cladding Strain as a Function of Fuel Enthalpy Increase and Fuel Radial Gap.

gap width which determines the time of gap contact and the cladding strain after gap contact, so that the enthalpy increase for the fuel failure by PCMI directly depends upon the fuel gap width before the transient. Therefore, it would be better to define the PCMI fuel failure criteria by the cladding strain or the fuel enthalpy increase during the transient rather than the total fuel enthalpy. Fig. 7 shows the cladding strain as a function of the fuel gap and the fuel enthalpy increase. By setting the cladding ductility versus burnup, boundary of threshold fuel enthalpy increase for fuel failure by PCMI can be determined. Results of CABRI Rep. Na-1 test that fuel failure may have occurred at the fuel enthalpy increase of about 15 cal/gm with the initial fuel enthalpy 15 cal/gm indicates that the cladding strain at fuel failure seems to be less than 0.2 % even assuming that fuel gap of test fuel rod is closed during pre-irradiation. It is somewhat consistent with the cladding burst test results by A. Garde[8] that ductility of the cladding with oxide spallation could be significantly reduced due to the local hydrogen concentration. Therefore, the fuel failure criteria for the high burnup fuel can be conservatively set as the enthalpy increase of as low as 7 cal/gm for the HFP case corresponding to the cladding strain of about 0.1 % at fuel gap closure as shown in Fig. 7 while the enthalpy increase of 15 cal/gm for the HZP case. The reason why fuel enthalpy increase for the HFP condition is less than that for the HZP condition is that for the HZP condition fuel gap before the transient is assumed to form due to the pellet thermal contraction as shown in Fig. 8 [9], but for the HFP condition fuel gap is assumed closed before the transient.

Fuel failure by DNB is another fuel failure mechanism under RIA condition. Even though test results[10] showed that occurrence of DNB does not immediately result in fuel failure, fuel failure has been conservatively assumed to occur right after DNB in the safety analysis. Fuel enthalpy at occurrence of DNB under RIA condition depends upon the fuel assembly design and the reactor thermal-hydraulic conditions during transient. For the 950 MWe Westinghouse-designed PWR the fuel enthalpy

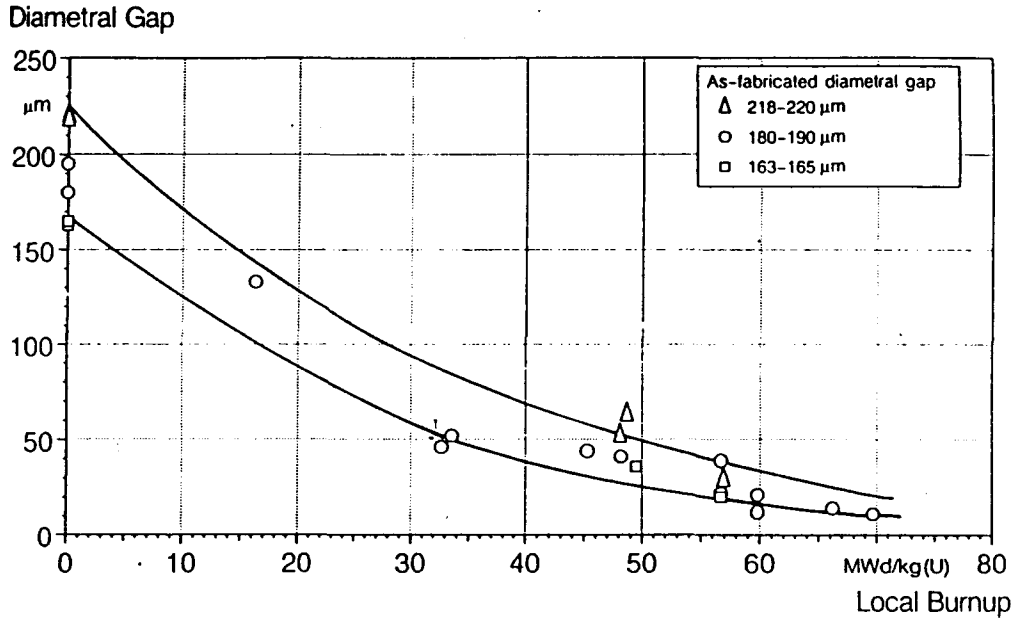

Fig. 8. Diametral Gap Between Fuel and Cladding as a Function of Local Burnup at Room Temperature[9]

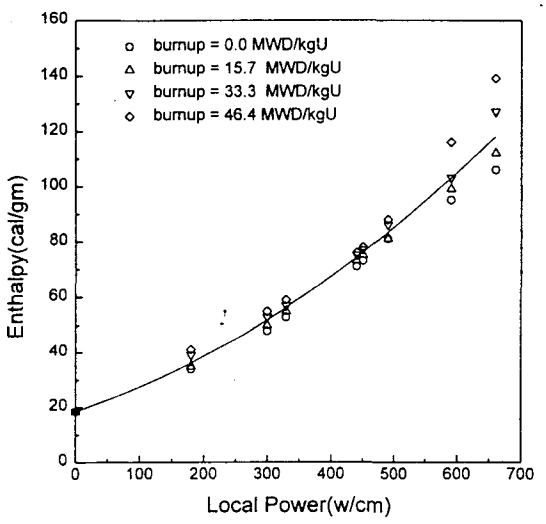

Fig. 9. Initial Fuel Enthalpy as a Function of the Fuel Rod Power Level.

at the power in which DNB is assumed to occur is estimated to be around 85 cal/gm. Fig. 9 shows the initial fuel enthalpy as a function of the fuel rod power level before the transient, where the scattering in the data point is mainly caused by the fuel gap conductance change with the burnup.

Then, by combining fuel failure limits by DNB and PCMI, fuel failure threshold with the burnup under RIA condition in PWR was tentatively determined. Table 2 shows the derived tentatively fuel failure criteria under RIA condition in PWR. Fuel failure by DNB occurs first at low burnup and at high burnup fuel failure occurs first by PCMI. Fuel failure by fuel centerline melting or fuel dispersion occurs at the fuel enthalpy far above these limits. Transition of first fuel failure mechanism from DNB to PCMI depends on the cladding ductility decrease with burnup which still needs to be more substantiated. Cladding ductility reduction by oxide spallation as well as cladding oxidation and fast neutron fluence, and maximum fuel gap

Table 3. Summary of the Results Performed for the Two PWR Fuel Loading Schemes.

Initial condition	Ejected rod worth($)	Peak total fuel enthalpy (cal/gm) / burnup (MWD/kgU)	Peak enthalpy increase (cal/gm) / burnup (MWD/kgU)	fuel failure fraction(%)
HZP	1.58	52.8 / 25.9	34.2 / 25.9	3.6
HFP	0.15	61.2 / 26.7	19.8 / 25.5	0.9

size decrease by cladding creep was assumed for the burnup higher than 30 MWD/kgU conservatively. For the burnup less than 30 MWD/kgU, total fuel enthalpy of 85 cal/gm in addition to DNB was set to cover the case that DNB occurs at the fuel enthalpy higher than 85 cal/gm. To get the more reliable fuel failure limit, it is clear that more test data need to be generated and evaluated. However, the uncertainty and insufficiency of the test data on the fuel failure by PCMI under RIA condition was compensated by the conservatism in the derivation of fuel failure criteria.

2.4 Results Analysis and Discussion

Analysis of the rod ejection accident was performed for the ultra low leakage and 18 month cycle length fuel loading scheme with a peak rod burnup of 68 MWD/kgU for the HZP and the HFP cases.

Figs. 10 and 11 exhibit the enthalpy increase and total enthalpy distribution in the core for the HZP and the HFP cases. The peak enthalpy increase occurred in the position where the control rod was ejected. It can be also seen that the higher burnup fuel has lower potential for the power increase during the rod ejection transient. As the distance from the ejected control rod increases, the magnitude of the enthalpy increase decreases significantly.

Fig. 12 shows the fractional distribution of the fuel burnup in the core where the groups of one, two and three-cycle burned fuel regions can be seen. Figs. 13 and 14 show the axial peak enthalpy increase versus the fuel rod burnup for the HZP and the HFP cases, respectively. From these results, the fraction of the fuel failure can be estimated by applying the fuel failure criteria versus the burnup. Fig. 15 shows that the distribution of the enthalpy increase is highly skewed to lower value and therefore, the fraction of the fuel failure would not be high during rod ejection accident.

Estimation of the fuel failure during the rod ejection accident as summarized in Table 3 showed 3.6 % fuel failure for the HZP and 0.9 % for the HFP when the newly derived fuel failure criteria given in Table 2 are applied. Since the peak radial average fuel enthalpy is 61.2 cal/gm for the HFP and 52.8 cal/gm for the HZP case, DNB is not expected to occur and the core damage design criteria would be adequately satisfied during the rod ejection accident.

Results of the conventional zero dimensional analysis showed that the peak radial average fuel enthalpy of 170 cal/gm for the HZP case and 98 cal/gm for the HFP case, and fuel failure by DNB is just below 10 %. When comparing those with the current three dimensional analysis results, the peak enthalpy and the peak enthalpy increase during the transient for the HZP case decreased by a factor of 3.2 and 4.4, respectively.

The conservatism employed in this analysis can

Fuel Enthalpy

.308	.711	1.307	1.712	1.165	.873	.737	.603	.741	.873	1.163	1.710	1.305	.710 *	.307
1.575	3.567	5.014	5.861	4.374	2.404	1.878	1.611	1.897	2.402	4.367	5.851	5.006	3.561	1.572
54.89	22.84	48.27	26.06	44.73	25.66	45.00	60.85	45.13	25.70	44.75	26.06	48.27	22.84	54.89
19.25	20.12	21.49	22.39	21.13	20.17	20.77	21.09	22.58	23.92	31.64	43.37	44.51	48.13	28.48
19.60	21.05	21.86	22.64	21.63	20.59	21.08	21.51	23.06	27.05	36.11	46.97	45.79	52.79	35.34
.303	1.119	1.668	1.224	1.142	.810	.758	.740	.759	.809	1.140	1.222	1.667	1.118	.303
1.880	4.841	5.923	4.458	4.180	2.711	2.047	1.891	2.048	2.707	4.173	4.450	5.918	4.836	1.879
51.47	20.33	25.26	60.04	41.57	46.09	45.01	45.12	45.06	46.13	41.59	60.05	25.27	20.35	51.50
19.24	21.02	22.30	21.31	21.18	20.56	20.89	21.46	22.72	24.89	31.10	35.33	47.81	44.26	26.48
19.80	21.92	22.63	21.47	21.55	20.75	21.13	22.00	23.50	22.37	35.35	39.29	51.48	51.74	34.65
	.647	1.302	1.685	.960	.673	.810	.873	.810	.672	.958	1.683	1.302	.649	
	3.610	4.889	5.167	3.758	2.623	2.708	2.402	2.708	2.621	3.749	5.611	4.885	3.610	
	52.76	43.65	24.86	57.99	24.85	46.11	25.70	46.12	24.86	58.06	24.86	43.68	52.87	
	20.01	21.47	22.42	20.89	20.40	21.10	21.13	22.64	23.44	28.08	38.72	36.91	29.36	
	20.91	21.91	22.67	21.31	21.16	21.71	22.41	23.35	26.25	31.73	42.49	40.69	37.00	
	.424	1.288	1.303	1.228	.959	1.141	1.164	1.141	.959	1.227	1.300	1.289	.440	
	2.743	4.845	4.510	3.982	3.753	4.175	4.368	4.174	3.753	3.978	4.504	4.844	2.782	
	50.38	19.27	40.25	40.84	58.06	41.58	44.75	41.58	58.00	40.85	40.35	19.32	46.78	
	19.50	21.31	21.43	21.69	21.44	22.48	23.16	24.18	24.60	28.30	36.92	32.99	24.28	
	20.42	22.18	21.90	22.27	22.28	23.57	24.37	25.47	25.94	31.39	35.08	37.72	30.14	
		.462	.947	1.302	1.684	1.222	1.710	1.222	1.683	1.301	.946	.460		
		2.331	2.996	4.507	5.615	4.452	5.854	4.452	5.610	4.504	2.992	2.335		
		52.59	20.05	40.35	24.85	60.05	26.06	60.04	24.86	40.26	20.05	52.64		
		19.49	20.17	22.00	23.87	22.95	25.63	24.44	28.06	26.59	23.77	22.56		
		20.27	21.19	22.87	24.51	23.56	26.34	25.13	28.88	27.53	27.08	26.27		
			.461	1.290	1.303	1.668	1.305	1.667	1.300	1.286	.462			
			2.337	4.847	4.888	5.921	5.008	5.915	4.883	4.839	2.328			
			52.66	19.32	43.68	25.27	48.27	25.26	43.65	19.27	52.59			
			19.66	22.20	22.83	24.71	24.01	26.46	25.40	25.67	21.16			
			20.63	23.41	23.63	25.39	25.03	27.43	26.52	27.81	23.31			
				.440	.650	1.119	.711	1.117	.646	.424				
				2.784	3.612	4.839	3.562	4.834	3.605	2.740				
				46.78	52.87	20.35	22.84	20.33	52.76	50.38				
				19.91	20.77	22.67	21.46	23.70	21.82	20.85				
				21.25	22.26	24.16	23.51	25.65	23.72	23.05				
						.303	.308	.303	- Initial FA Avg. Fxy					
						1.880	1.53	1.878	- Initial Local Peak Fxyz					
						51.51	54.89	51.47	- FA Avg. Burnup(MWD/kgU)					
						19.71	19.83	19.92	- FA Avg. Enthalpy(cal/gm)					
						20.66	20.60	21.10	- Local Max. Enthalpy(cal/gm)					

(*) The position in which a D-bank control rod is ejected

Fuel Enthalpy Increase

.308	.711	1.307	1.712	1.165	.873	.737	.603	.741	.873	1.163	1.710	1.305	.710 *	.307
1.575	3.567	5.014	5.861	4.374	2.404	1.878	1.611	1.897	2.402	4.367	5.851	5.006	3.561	1.572
54.89	22.84	48.27	26.06	44.73	25.66	45.00	60.85	45.13	25.70	44.75	26.06	48.27	22.84	54.89
.65	1.52	2.89	3.79	2.53	1.57	2.17	2.49	3.98	5.32	13.04	24.77	25.91	29.53	9.88
1.00	2.45	3.26	4.04	3.03	1.99	2.48	2.91	4.46	8.45	17.51	28.37	27.19	34.19	16.74
.303	1.119	1.668	1.224	1.142	.810	.758	.740	.759	.809	1.140	1.222	1.667	1.118	.303
1.880	4.841	5.923	4.458	4.180	2.711	2.047	1.891	2.048	2.707	4.173	4.450	5.918	4.836	1.879
51.47	20.33	25.26	60.04	41.57	46.09	45.01	45.12	45.06	46.13	41.59	60.05	25.27	20.35	51.50
.64	2.42	3.70	2.71	2.58	1.96	2.29	2.86	4.12	6.29	12.50	16.73	29.21	25.66	7.88
1.20	3.32	4.03	2.87	2.95	2.15	2.53	3.40	4.90	8.77	16.75	20.69	32.88	33.14	16.05
	.647	1.302	1.685	.960	.673	.810	.873	.810	.672	.958	1.683	1.302	.649	
	3.610	4.889	5.167	3.758	2.623	2.708	2.402	2.708	2.621	3.749	5.611	4.775	3.610	
	52.76	43.65	24.86	57.99	24.85	46.11	25.70	46.12	24.86	58.06	24.86	43.68	52.87	
	1.41	2.87	3.82	2.29	1.80	2.50	2.53	4.04	4.84	9.48	20.12	18.31	10.76	
	2.31	3.31	4.07	2.71	2.56	3.11	3.81	4.75	7.65	13.13	23.89	22.09	18.40	
	.424	1.288	1.303	1.228	.959	1.141	1.164	1.141	.959	1.227	1.300	1.289	.440	
	2.743	4.845	4.510	3.982	3.753	4.175	4.368	4.174	3.753	3.978	4.504	4.844	2.782	
	50.38	19.27	40.25	40.84	58.06	41.58	44.75	41.58	58.00	40.85	40.35	19.32	46.78	
	.90	2.71	2.83	3.09	2.84	3.88	4.56	5.58	6.00	9.70	12.32	14.49	5.68	
	1.82	3.58	3.30	3.67	3.68	4.97	5.77	6.87	7.34	12.79	16.48	19.12	11.54	
		.462	.947	1.302	1.684	1.222	1.710	1.222	1.683	1.301	.946	.460		
		2.331	2.996	4.507	5.615	4.452	5.854	4.452	5.610	4.504	2.992	2.335		
		52.59	20.05	40.35	24.85	60.05	26.06	60.04	24.86	40.26	20.05	52.64		
		.89	1.57	3.40	5.27	4.35	7.03	5.84	9.46	7.99	5.17	3.96		
		1.67	2.59	4.27	5.91	4.96	7.74	6.53	10.28	8.93	8.48	7.67		
			.461	1.290	1.303	1.668	1.305	1.667	1.300	1.286	.462			
			2.337	4.847	4.888	5.921	5.008	5.915	4.883	4.839	2.328			
			52.66	19.32	43.68	25.27	48.27	25.26	43.65	19.27	52.59			
			1.06	3.60	4.23	6.11	5.41	7.86	6.80	7.07	2.56			
			2.03	4.81	5.03	6.79	6.43	8.83	7.92	24.08	4.71			
				.440	.650	1.119	.711	1.117	.646	.424				
				2.784	3.612	4.839	3.562	4.834	3.605	2.740				
				46.78	52.87	20.35	22.84	20.33	52.76	50.38				
				1.31	2.17	4.07	2.86	5.10	3.22	2.25				
				2.65	3.66	5.56	4.91	7.05	5.12	4.45				
						.303	.308	.303	- Initial FA Avg. Fxy					
						1.880	1.673	1.878	- Initial Local Peak Fxyz					
						51.51	54.89	51.47	- FA Avg. Burnup(MWD/kgU)					
						1.11	1.23	1.32	- FA Avg. Enthalpy Increase(MWD/kgU)					
						2.06	2.00	2.50	- Local Max. Enthalpy Increase(cal/gm)					

(*)The position in which a D-bank control rod is ejected

Fig. 10. Fuel Enthalpy Increase Distribution in the Core After the HZP Rod Ejection Transient at EOC.

Fuel Enthalpy

.393	1.096	1.145	1.427	1.187	1.401	1.074	.869	1.079	1.401	1.187	1.426	1.145	1.096 *	.393
.846	1.723	1.460	1.763	1.463	1.743	1.362	1.056	1.363	1.743	1.463	1.762	1.460	1.723	.846
54.89	22.84	48.27	26.06	44.73	25.66	45.00	60.85	45.13	25.70	44.75	26.06	48.27	22.84	54.89
23.00	29.09	40.97	51.23	45.36	50.02	42.67	37.83	43.75	52.47	49.10	58.35	50.80	46.56	28.82
25.76	36.73	44.59	52.96	46.40	51.97	44.32	38.41	45.75	54.88	50.96	60.70	52.72	52.17	35.20
.338	1.097	1.378	1.028	1.161	1.116	1.091	1.078	1.092	1.116	1.160	1.028	1.378	1.097	.338
.823	1.732	1.768	1.297	1.456	1.421	1.359	1.363	1.361	1.420	1.455	1.296	1.764	1.732	.823
51.47	20.33	25.26	60.04	41.57	46.09	45.01	45.12	45.06	46.13	41.59	60.05	25.27	20.35	51.50
22.90	37.34	48.33	41.09	43.47	40.40	41.86	43.13	42.69	42.14	46.84	45.93	58.01	48.36	27.05
27.45	45.11	51.92	41.83	45.74	43.95	43.07	44.77	44.17	46.17	50.23	47.72	61.15	57.38	35.30
	.562	1.051	1.405	.984	1.231	1.116	1.401	1.116	1.231	.983	1.404	1.052	.565	
	1.070	1.394	1.701	1.245	1.707	1.421	1.743	1.421	1.707	1.243	1.700	1.394	1.070	
	52.76	43.65	24.86	57.99	24.85	46.11	25.70	46.12	24.86	58.06	24.86	43.68	52.87	
	29.76	42.96	51.86	37.74	32.41	40.62	50.62	41.18	33.40	40.05	57.05	48.58	33.86	
	36.93	46.61	54.32	41.26	36.87	44.32	52.63	44.62	38.59	44.25	60.01	52.76	43.56	
	.377	1.129	1.190	1.164	.984	1.161	1.187	1.161	.984	1.164	1.188	1.130	.392	
	.876	1.611	1.461	1.416	1.243	1.455	1.463	1.455	1.244	1.416	1.458	1.610	.888	
	50.38	19.27	40.25	40.84	58.06	41.58	44.75	41.58	58.00	40.85	40.35	19.32	46.78	
	26.05	45.30	46.89	44.60	37.84	43.80	45.94	44.34	38.87	46.82	50.26	49.56	28.27	
	34.40	53.80	48.24	47.40	41.38	46.17	47.06	46.56	42.68	49.89	52.32	58.95	38.57	
		.493	1.191	1.188	1.404	1.028	1.426	1.028	1.404	1.189	1.191	.491		
		1.072	1.659	1.458	1.700	1.297	1.762	1.297	1.700	1.460	1.658	1.075		
		52.59	20.05	40.35	24.85	60.05	26.06	60.04	24.86	40.26	20.05	52.64		
		28.84	47.27	46.98	52.12	41.42	51.94	41.87	53.43	48.79	49.80	30.24		
		38.99	55.23	48.39	54.57	42.12	53.69	42.77	56.11	50.02	58.32	41.55		
			.491	1.130	1.052	1.378	1.145	1.377	1.051	1.128	.493			
			1.075	1.610	1.394	1.764	1.460	1.767	1.393	1.611	1.072			
			52.66	19.32	43.68	25.27	48.27	25.26	43.65	19.27	52.59			
			28.85	45.52	43.24	48.78	41.48	49.26	44.05	46.83	29.70			
			39.05	53.99	46.92	52.33	45.21	53.04	47.89	55.68	40.49			
				.392	.565	1.097	1.096	1.096	.562	.377				
				.888	1.070	1.732	1.723	1.732	1.069	.875				
				46.78	52.87	20.35	22.84	20.33	52.76	50.38				
				26.42	29.97	37.67	29.37	37.95	30.28	26.51				
				34.95	37.19	45.52	37.23	45.92	37.63	35.23				
						.338	.393	.338						
						.823	.846	.823						
						51.51	54.89	51.47						
						23.00	23.13	23.07						
						27.63	26.00	27.76						

(*) The position in which a D-bank control rod is ejected.

- Initial FA Avg. Fxy
- Initial Local Peak Fxyz
- FA Avg. Burnup(MWD/kgU)
- FA Avg. Enthalpy(cal/gm)
- Local Max. Enthalpy(cal/gm)

Fuel Enthalpy Increase

.393	1.096	1.145	1.427	1.187	1.401	1.074	.869	1.079	1.401	1.187	1.426	1.145	1.096 *	.393
.846	1.723	1.460	1.763	1.463	1.743	1.362	1.056	1.363	1.743	1.463	1.762	1.460	1.723	.846
54.89	22.84	48.27	26.06	44.73	25.66	45.00	60.85	45.13	25.70	44.75	26.06	48.27	22.84	54.89
.09	.67	.92	1.66	2.24	2.67	2.35	2.31	3.13	4.68	4.36	6.85	9.30	17.17	5.77
.14	1.45	2.09	2.63	2.31	2.80	2.40	2.39	3.57	5.28	5.11	8.26	13.10	19.84	10.50
.338	1.097	1.378	1.028	1.161	1.116	1.091	1.078	1.092	1.116	1.160	1.028	1.378	1.097	.338
.823	1.732	1.768	1.297	1.456	1.421	1.359	1.363	1.361	1.420	1.455	1.296	1.764	1.732	.823
51.47	20.33	25.26	60.04	41.57	46.09	45.01	45.12	45.06	46.13	41.59	60.05	25.27	20.35	51.50
.14	1.01	1.05	.99	2.11	2.02	2.30	2.63	2.95	3.47	4.04	4.77	9.03	10.39	3.98
.30	2.11	2.43	1.93	2.24	2.27	2.47	2.80	3.40	4.38	4.93	6.27	12.38	15.22	8.84
	.562	1.051	1.405	.984	1.231	1.116	1.401	1.116	1.231	.983	1.404	1.052	.565	
	1.070	1.394	1.701	1.245	1.707	1.421	1.743	1.421	1.707	1.243	1.700	1.394	1.070	
	52.76	43.65	24.86	57.99	24.85	46.11	25.70	46.12	24.86	58.06	24.86	43.68	52.87	
	.21	1.38	1.98	1.72	1.41	2.19	3.14	2.65	2.25	3.30	5.12	5.39	3.85	
	.42	2.22	2.67	1.93	1.83	2.55	3.32	2.83	3.29	4.26	6.51	6.77	6.25	
	.377	1.129	1.190	1.164	.984	1.161	1.187	1.161	.984	1.164	1.188	1.130	.392	
	.876	1.611	1.461	1.416	1.243	1.455	1.463	1.455	1.244	1.416	1.458	1.610	.888	
	50.38	19.27	40.25	40.84	58.06	41.58	44.75	41.58	58.00	40.85	40.35	19.32	46.78	
	.15	1.90	2.19	2.18	1.81	2.39	2.72	2.83	2.67	4.04	4.18	4.19	1.94	
	.28	2.64	2.34	2.35	2.06	2.60	2.53	3.02	3.14	4.83	5.16	5.29	3.71	
		.493	1.191	1.188	1.404	1.028	1.426	1.028	1.404	1.189	1.191	.491		
		1.072	1.659	1.458	1.700	1.297	1.762	1.297	1.700	1.460	1.658	1.075		
		52.59	20.05	40.35	24.85	60.05	26.06	60.04	24.86	40.26	20.05	52.64		
		.25	2.27	2.35	2.76	2.17	3.09	2.55	3.83	3.84	4.36	1.73		
		.41	2.79	2.46	2.90	2.27	3.36	2.71	4.16	4.32	5.32	3.52		
			.491	1.130	1.052	1.378	1.145	1.377	1.051	1.128	.493			
			1.075	1.610	1.394	1.764	1.460	1.767	1.393	1.611	1.072			
			52.66	19.32	43.68	25.27	48.27	25.26	43.65	19.27	52.59			
			.34	2.26	2.19	2.66	2.29	3.07	2.89	3.39	1.74			
			.61	2.81	2.46	2.92	2.67	3.45	3.40	4.19	3.02			
				.392	.565	1.097	1.096	1.096	.562	.377				
				.888	1.070	1.732	1.723	1.732	1.069	.875				
				46.78	52.87	20.35	22.84	20.33	52.76	50.38				
				.73	1.18	1.85	1.24	2.11	1.50	1.17				
				1.40	1.80	2.44	2.00	2.81	2.18	2.12				
						.338	.393	.338						
						.823	.846	.823						
						51.51	54.89	51.47						
						.58	.63	.65						
						1.03	.95	1.16						

(*) The position in which a D-bank control rod is ejected.

- Initial FA Avg. Fxy
- Initial Local Peak Fxyz
- FA Avg. Burnup(MWD/kgU)
- FA Avg. Enthalpy Increase(cal/gm)
- Local Max. Enthalpy Increase (cal/gm)

Fig. 11. Fuel Enthalpy Increase Distribution in the Core After the HFP Rod Ejection Transient at EOC.

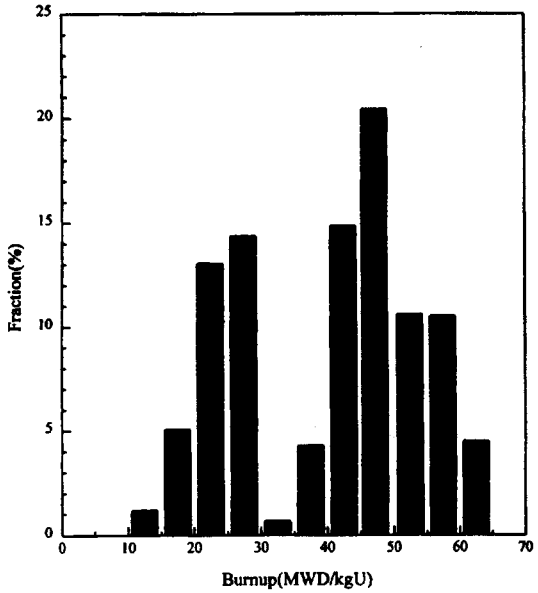

Fig. 12. Fractional Distribution of the Fuel Burnup in the Core

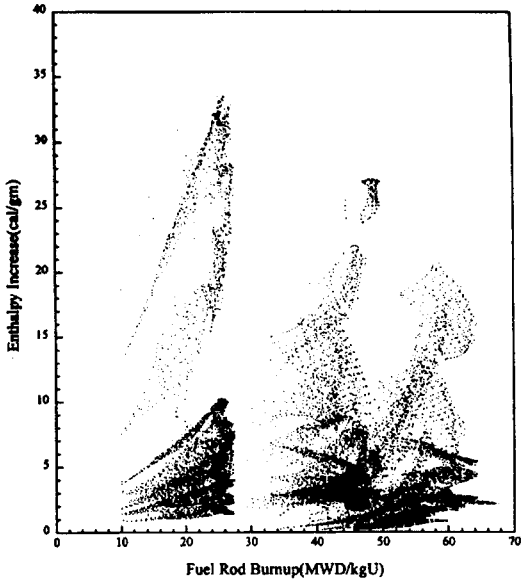

Fig. 13. Fuel Enthalpy Increase Versus Fuel Rod Burnup After the HZP Rod Ejection Transient at EOC.

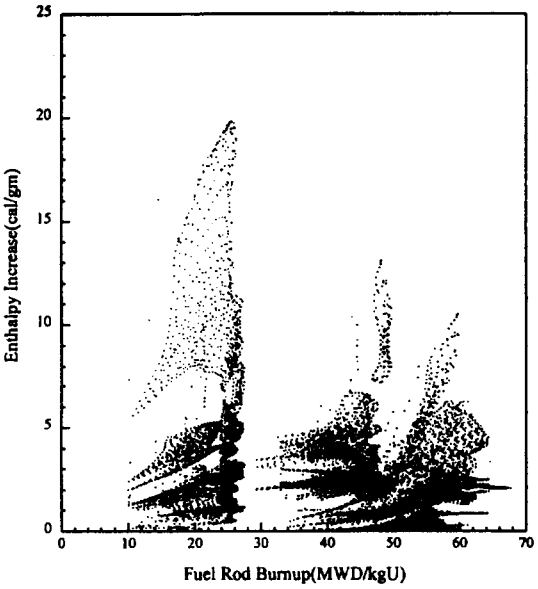

Fig. 14. Fuel Enthalpy Increase Versus Fuel Rod Burnup After the HFP Rod Ejection Transient at EOC.

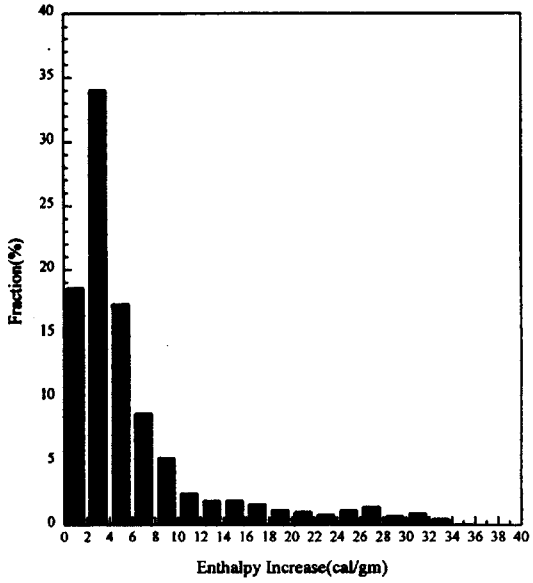

Fig. 15. Fractional Distribution of Fuel Enthalpy Increase After the HZP Rod Ejection Transient at EOC.

be summarized as follows. The core conditions and assumptions used in the transient power calculation are kept conservative as same as the conventional safety analysis. The assumption of adiabatic enthalpy increase during the transient over-estimates the enthalpy increase conservatively. The derived fuel failure criteria can be considered conservative because the fuel property degradation at the high burnup of over 60 MWD/kgU is assumed to occur as early as 30 MWD/kgU. Therefore, it can be said that the fractional fuel failure during both the HZP and the HFP rod ejection accidents is less than 10 % which is an upper limit of the current safety analysis even assuming the conservative fuel failure criteria, and the coolable geometry of the core would be still maintained.

3. Conclusions

- Fuel behavior under the rod ejection accident in a typical Westinghouse-designed 950 MWe PWR plant was analyzed through the three dimensional transient core power calculation with the nodal neutronics code, PANBOX2 and the transient fuel rod analysis code, FRAP-T6.
- Tentative fuel failure design criteria were newly derived, using the available simulated RIA test results in the research reactors and the FRAP-T6 prediction. The fuel failure limits by PCMI mechanism were defined in terms of fuel enthalpy increase during the transient instead of total fuel enthalpy. Even though more test data are necessary to set the reliable fuel failure limit, the uncertainties were compensated by the conservative determination of the fuel failure limit.
- Results of three-dimensional analysis of the rod ejection accident in the core of the high burnup and longer cycle length fuel loading scheme with the peak rod burnup of over 60 MWD/kgU by keeping the same conservative assumptions of the conventional zero dimensional analysis methodology and applying the newly derived conservative fuel failure criteria showed that the fuel failure would be less than 4 % and the peak fuel enthalpy would be 61.2 cal/gm. Therefore, it is expected that the assumption of 10 % fuel failure during the rod ejection accident in the current safety analysis would be still bounding and the core coolable geometry would be still maintained.

References

1. P.E. Macdonald et al., "Assessment of Light-water-reactor fuel damage during a reactivity-initiated accident", Nuclear Safety, vol.21-No.5, (1980).
2. F. Schmitz et al., "Investigation of the behavior of high burnup PWR fuel under RIA conditions in the CABRI test reactor", 22nd Water Reactor Safety Information Meeting, October 24-26, (1994).
3. R. Boeer et al., "Code Manual PANBOX 2.2, Rev. c", Siemens/KWU Technical Report, BT25/92/E516, (1992).
4. R. Boeer and H. Rascher, "PANBOX2 Results of NEACRP PWR Rod Ejection Benchmark Calculations and Comparisons with PANBOX1 and PANTHER", Siemens/KWU Work Report BT12/1994/ E427, (1994).
5. L.J. Siefken et al., "FRAP-T6 : A computer code for the transient analysis of oxide fuel rods", NUREG/CR-2148, (1981).
6. T. Fuketa et al., Behavior of High Burnup PWR Fuel Under a Simulated RIA Condition in the NSRR, OECD Specialist Meeting on Transient Behavior of High Burnup Fuel, Cadarache, France, 12-14 Sept. (1995).

7. J. Papin et al, The behavior of irradiated fuel under RIA transients : interpretation of the CABRI experiments, OECD Specialist Meeting on Transient Behavior of High Burnup Fuel, Cadarache, France, 12-14 Sept. (1995).
8. A. Garde et al., Effects of hydride precipitate localization and neutron fluence on the ductility of irradiated Zircaloy-4, Zirconium in the Nuclear Industry : Eighth International Symposium, ASTM STP 1295, Sept. 11-14, (1995).
9. R. Manzel, et al., "Fuel rod behavior at extended burnup", Proc. of 1994 Int. Top. Meeting on LWR Fuel Performance, West Palm Beach, Florida, April 17-21, (1994).
10. R. V. Houten, Fuel Rod Failure as a Consequence of Departure from Nucleate Boiling or Dryout, NUREG-0562, USNRC, (1979).